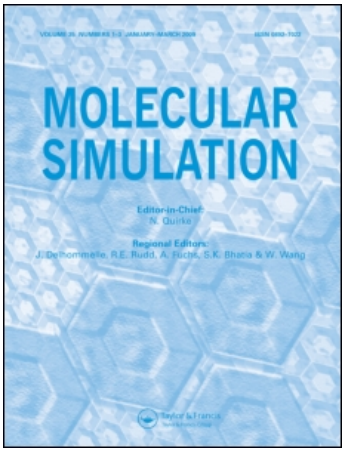

Molecular Simulation
Publication details, including instructions for authors and subscription information:
http://www.informaworld.com/smpp/title~content=t713644482

Molecular Dynamics Simulation Studies of the Limiting Conductances of $CaCl_2$ using Extended Simple Point Charge and Revised Polarizable Models

Song Hi Lee[a]
[a] Department of Chemistry, Kyungsung University, Pusan, South Korea

To cite this Article Lee, Song Hi(2004) 'Molecular Dynamics Simulation Studies of the Limiting Conductances of $CaCl_2$ using Extended Simple Point Charge and Revised Polarizable Models', Molecular Simulation, 30: 10, 669 — 678
To link to this Article: DOI: 10.1080/08927020412331279910
URL: http://dx.doi.org/10.1080/08927020412331279910

Molecular Simulation, VOL. 30 (10), 30 August 2004, pp. 669–678

Taylor & Francis
Taylor & Francis Group

Molecular Dynamics Simulation Studies of the Limiting Conductances of $CaCl_2$ using Extended Simple Point Charge and Revised Polarizable Models

SONG HI LEE*

Department of Chemistry, Kyungsung University, Pusan 608-736, South Korea

(Received June 2004; In final form June 2004)

We have carried out molecular dynamics (MD) simulations of the limiting conductances of $CaCl_2$ in ambient and supercritical states as a function of water density using extended simple point charge (SPC/E) and revised polarizable (RPOL) models for ions and water molecules. Both models predict the limiting conductances of $CaCl_2$ in supercritical water that are a linear dependence on water density. The effect of the electronic polarization on the limiting conductances is too small to cause a deduction in the lower water density of 0.6 ~ 0.7 g/cc in this study. The most significant effect of the electronic polarization is appeared in a decrease in the ion–water potential energy and, as a result, an increase in the limiting conductances for both ions. Different charge distributions of water molecules in the first hydration shell around the ions lead the opposite behavior of the induced dipole moment with water density for a positive and a negative ion in supercritical water; the induced dipole moment of Ca^{2+} decreases with increasing water density but for Cl^-, the opposite is observed. The same kind of opposite behavior due to the structure of water molecules around the ions is also found in hydrogen-bond correlations of water around the ions and of bulk water; hydrogen bonding around Ca^{2+} persists longer than in bulk water whereas the opposite is observed for Cl^-.

Keywords: Molecular dynamics; Simple point charge; Revised polarizable; Conductance

INTRODUCTION

Two experimental results [1,2] of the limiting equivalent conductances as a function of water density in supercritical water showed two different trends: Wood *et al.* [1] reported a clear change of slope from the assumed linear dependence of limiting equivalent conductances of LiCl, NaCl, NaBr, and CsBr on water density, and on the other hand, a clear maximum in limiting equivalent conductances of NaOH reported by Ho and Palmer [2]. The clear change of the slope from the assumed linear dependence of the limiting equivalent conductances of NaCl on water density is located around 0.45 g/cc and the maximum in the limiting equivalent conductances of NaOH is located around 0.55 g/cc.

Recently, Frantz and Marshall [3] measured the electrical conductances of $MgCl_2$ and $CaCl_2$ in dilute aqueous solutions from 25 to 600 C at pressures up to 4000 bars. Solution compositions of the salts used were between 0.001 and 0.005 m. The results showed that in $MgCl_2$ and $CaCl_2$ solutions with compositions less than 0.005 m the salts exist primarily as Mg^{2+}, Ca^{2+}, and Cl^- ions at temperatures below 400 C and densities greater than 0.75 g/cc. They computed the limiting equivalent conductances in this temperature–density range. Figure 1 shows the limiting equivalent conductances of $CaCl_2$ (0.001 m) as a function of water density below 400 C where a clear maximum is located around 0.8 g/cc.

In a previous study [4], we have reported results of molecular dynamics (MD) simulations of the limiting conductances of $MgCl_2$ and $CaCl_2$ in supercritical water as a function of water density using the extended simple point charge (SPC/E) model [5] for ions and water molecules. The limiting conductances of Mg^{2+}, Ca^{2+} and Cl^- over the whole range of water density considered exhibited a linear dependence of the limiting conductance on water density.

*E-mail: shlee@star.ks.ac.kr

ISSN 0892-7022 print/ISSN 1029-0435 online © 2004 Taylor & Francis Ltd
DOI: 10.1080/08927020412331279910

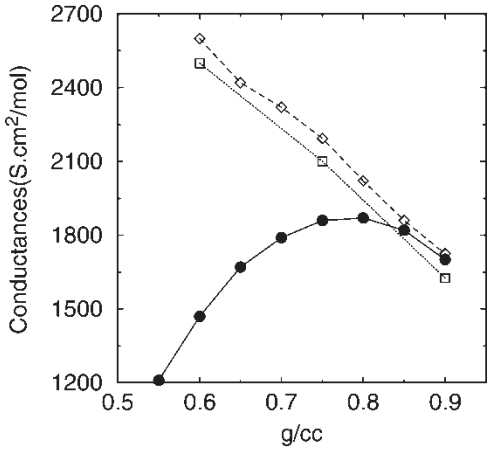

FIGURE 1 Comparison of the limiting molar conductances of $CaCl_2$ at infinite dilution as a function of density of supercritical water at 673 K obtained from MSD's using the SPC/E (open squares) and RPOL models (open diamonds) with the experimental results (filled circles) [3].

In the cases of Mg^{2+} and Ca^{2+}, a solventberg picture for the behavior of small divalent cation emerged from this study. From the view of the solventberg picture, the ion and its shell moving together as an entity interacts with water molecules in the second hydration shell, and its mobility is restricted mostly by the number of the second hydration shell water which is proportional to water density of the whole system. In the case of Cl^-, the range of water density considered in this study belongs to the higher-density region (above 0.45 g/cc) in which the effect of the number of hydration water molecules around ions dominated. As water density increases, the water molecules of the first hydration shell restrict the mobility of Cl^- and the limiting conductance of Cl^- decreases nearly linearly. Significant different dependence on water density was observed between the calculated limiting conductances of $MgCl_2$ and $CaCl_2$ at 673 K and the experimental results over the water density of range 0.60–0.90 g/cc. Possible limitation of the extended SPC/E model [5] with regard to this difference was pointed out.

In this paper, we extend our MD simulations to the system of $CaCl_2$ in ambient and supercritical states using the revised polarizable (RPOL) model [6,7] for ions and water molecules. The study for this system is in conjunction with our previous studies of NaCl to delineate the effect of charge doubling [8] and of $MgCl_2$ and $CaCl_2$ by the use of the SPC/E model for water [4]. The application of Ewald summation [9] to the use of the RPOL model [6,7] for ions and water molecules in dilute aqueous solutions of $CaCl_2$ will be the next subject in our series of studies on ionic systems [4,8,10–17]. In the following section, we describe the technical details of MD simulation. We present our results in third section and the concluding remarks in fourth section.

MOLECULAR MODELS AND MOLECULAR DYNAMICS SIMULATION DETAILS

It is now widely accepted that many-body or non-additive interactions are important if one wishes to quantitatively describe ionic interactions [6,7,18–29]. The first polarizable potential model that explicitly includes the electronic polarization energy by the use of MD method is the polarizable (POL1) model of Caldwell *et al.* [24,25].

The RPOL model [6,7] consists of the Lennard-Jones (LJ) and electrostatic interactions, plus a non-additive polarization energy. The ion is represented by a point-charge model including the polarizability placed on the LJ center. The total potential of the system, which does not include the 3-body interaction [24,25,27], is given by

$$U_{\text{tot}} = U_{\text{pair}} + U_{\text{pol}}. \tag{1}$$

The pair-additive potential is

$$U_{\text{pair}} = \sum_i \sum_j \left\{ 4\varepsilon \left[\left(\frac{\sigma_{ij}}{r_{ij}} \right)^{12} - \left(\frac{\sigma_{ij}}{r_{ij}} \right)^{6} \right] - \frac{q_i q_j}{r_{ij}} \right\} \tag{2}$$

and the polarization energy is

$$U_{\text{pol}} = -\frac{1}{2} \sum_i \mu_i \cdot \mathbf{E}_i^o \tag{3}$$

where μ_i is the induced dipole moment, and $\boldsymbol{E}_i^o$ is the electrostatic field at atom i. During the MD simulation, the induced dipole moment μ_i and the total electrostatic field $\boldsymbol{E}_i$ at the polarizable center are evaluated by the self-consistent-field method using following expressions:

$$\mu_i = \alpha_i \, \mathbf{E}_i \tag{4}$$

$$\mathbf{E}_i = \mathbf{E}_i^o + \sum_{j=1, j \neq i} \mathbf{T}_{ij} \cdot \mu_j \tag{5}$$

$$\mathbf{E}_i^o = \sum_{j=1, j \neq i} q_j \frac{\mathbf{r}_{ij}}{\boldsymbol{r}_{ij}^3} \tag{6}$$

and

$$\mathbf{T}_{ij} = \frac{1}{\boldsymbol{r}_{ij}^3} \left(\frac{3 \mathbf{r}_{ij} \mathbf{r}_{ij}}{\boldsymbol{r}_{ij}^2} - \mathbf{U} \right) \tag{7}$$

where $\mathbf{T}_{ij}$ is the dipole tensor, α_i the polarizability of atom i, $\mathbf{r}_{ij}$ the vector from atom j to i, q_j is the charge at atom j, and $\mathbf{U}$ is the unit tensor. To solve Eqs. (4) and (5), the traditional iterative approach was used with the iteration continuing until the root mean square of the difference in the induced dipole moment between successive iterations was less than 0.01 D/atom. The self-consistency was usually achieved within five iterative steps.

The potential parameters of the RPOL model for ions and water molecules without the 3-body

TABLE I Comparison of potential parameters for the SPC/E and RPOL models without three-body interaction. σ(A) and ε(kJ/mol)

Model	*Atom and ion*	σ_{OO} *and* σ_{iO}	ε_{OO} *and* ε_{iO}	*q (e)*	α *(A^3)*	*References*
SPC/E	O of H_2O	3.169	0.6502	−0.8476	–	[5]
	H of H_2O	–	–	+0.4238	–	[5]
	Cl^-	3.785	0.5216	−1	–	[11,12]
	Ca^{2+}	3.019	0.5216	+2	–	[43]
	Ca^{2+}	2.38*	147*	+2	–	[4]
RPOL	O of H_2O	3.196	0.6694	−0.730	0.528	[6]
	H of H_2O	–	–	+0.365	0.170	[6]
	Cl^-	3.823	0.5292	−1	3.250	[7]
	Ca^{2+}	3.019	0.5216	+2	0.5†	[43]

* Trial values used in Ref. [4]. † A trial value used in Ref. [4] and in this study.

interaction are compared with SPC/E model [5] in Table I. The LJ parameters for Ca^{2+} used in Ref. [4] were deduced from Ca^{2+}–water pair potential [30] calculated with $V_{Ca-O}(r)$ and $V_{Ca-H}(r)$ pair potentials, whose derivation was based on *ab initio* calculations of different ion–water configurations. A spherical cut-off r_c of half the simulation box length was employed for all the pair interactions. This is a simple truncation in which two molecules are considered as interacting if the distance between their centers is less than the cut-off radius r_c and the interaction is neglected if the distance is larger than r_c. This simple truncation of all interactions for water containing a single ion was shown by Perera *et al.* [31] to be comparable in accuracy to the use of Ewald summation [9] or reaction field methods [32].

The experimental critical properties of water are $T_c = 647.13\,\text{K}$, $\rho_c = 0.322\,\text{g/cc}$, and $P_c = 220.55\,\text{bar}$ [33] and the critical properties of SPC/E water are $T_c = 640\,\text{K}$, $\rho_c = 0.29\,\text{g/cc}$, and $P_c = 160\,\text{bar}$ [34]. We chose the simulation state points for the calculation of the limiting conductance of Ca^{2+} and Cl^- ions, $T_r = T/T_c = 1.05\,(673\,\text{K})$ and at the reduced densities, $\rho_r = \rho/\rho_c = 2.07, 2.24, 2.41, 2.59, 2.76, 2.93$, and 3.10, corresponding to real densities of about 0.6, 0.65, 0.7, 0.75, 0.8, 0.85, and 0.9 g/cc for the SPC/E model; this spans the range of densities around 0.75–0.8 g/cc where the maximum in the limiting equivalent conductances of $CaCl_2$ are located around 0.75–0.8 g/cc. [33]

We used Gaussian isokinetics [35–38] to keep the temperature of the system constant and the quaternion formulation [39,40] of the equations of rotational motion about the center of mass of water molecule. For the integration over time, we adopted Gear's fifth-order predictor–corrector algorithm [41,42] with a time step of $0.5 \times 10^{-15}\,\text{s}$ (0.5 fs). Each MD simulation of a single ion system with 215 water molecules were carried out for Ca^{2+} and Cl^- for 2,000,000 time steps after equilibration of 1,000,000 time steps. The equilibrium properties are averaged over 10 blocks of 200,000 time steps and the configurations of water molecules and an ion are stored every 10 time steps for further analysis.

The diffusion coefficient, D_i, of each ion is calculated from the mean square displacement (MSD) and from the velocity auto-correlation function (VAC), and the ion mobility is obtained by

$$u_i = D_i z_i e/k_B T = D_i z_i F/RT \quad \text{(Einstein relation)}$$

where k_B is the Boltzmann constant, R is the gas constant, F is the Faraday constant, z_i is the charge on the ion in units of the electronic charge e, T is the absolute temperature, and $i = +$ and $-$. The limiting conductance of each ion can be calculated from

$$\lambda_i^o = u_i\, z_i\, F = D_i z_i^2 F^2/RT \tag{8}$$

The total limiting conductance of a salt is the sum of contributions from its individual ions : $\lambda^o = \nu_+\lambda_+^o + \nu_-\lambda_-^o$, where ν_+ and ν_- are the numbers of cations and anions per formula unit of electrolyte (e.g. $\nu_+ = 1$ and $\nu_- = 2$ for $CaCl_2$).

RESULTS AND DISCUSSION

In order to carry out the MD simulation for the RPOL model, the first task is to determine the polarizabilities for atoms of water molecule and for ions. Table II lists the polarizabilities used in MD simulations and found in the literatures. The magnitude of the induced dipole moment is proportional to the strength of the applied electric field defined by Eq. (4), where the constant is the polarizability of the molecule. The larger the polarizability of the molecule, the greater the distortion that is caused by a given electric field. If the molecule has few electrons, they are tightly controlled by the nuclear charges and the polarizability of the molecule is low. If the molecule contains large atoms with electrons some distance from the nucleus, the nuclear control is less, the electron distribution is flabbier, and the polarizability is greater. The polarizability of Ca^{2+} is hardly found in the literature but is chosen as $0.5\,\text{A}^3$. The potential parameters of the SPC/E and RPOL models for water, Cl^- and Ca^{2+} ions without the 3-body interaction used in this study are listed in Table I.

TABLE II Polarizability

	Atom and ion	*α* (A^3)	*References*		*Atom and ion*	*α* (A^3)
With 3-body	O of H_2O	0.465	[25]	Ref. [19]	F^-	0.9743
	H of H_2O	0.135			Cl^-	3.2350
	Na^+	0.25	[25]		Br^-	4.5330
	Cl^-	3.25	[25]		I^-	6.7629
	Li^+	0.029	[27]	Ref. [44]	Li^+	0.029
	F^-	0.974	[27]		Na^+	0.179
Without 3-body	O of H_2O	0.528	[28]		K^+	0.83
	H of H_2O	0.170			Rb^+	1.40
	I^-	6.902	[28]		Cs^+	2.42
	I	5.500	[28]		F^-	1.04
	Cl^-	3.690	[29]		Cl^-	3.66
	Cl	2.180	[29]		Br^-	4.77
	Na^+	0.24	[7]		I^-	7.1
	Cl^-	3.25	[7]		Be^{2+}	0.008
Ref. [19]	Li^+	0.029			Mg^{2+}	0.094
	Na^+	0.2495			Ca^{2+}	0.47
	K^+	1.0571			Sr^{2+}	0.86
	Rb^+	1.5600			Ba^{2+}	1.55
	Cs^+	2.5880			Ca^{2+}	0.5*

*A trial value used in this study.

Figures 2 and 3 show ion–oxygen $g_{i-O}(r)$ and ion–hydrogen $g_{i-H}(r)$ radial distribution functions for Ca^{2+} and Cl^- ions at 673 K over the water densities of 0.60 and 0.90 g/cc A tall, sharp peak in $g_{Ca-O}(r)$ corresponding to the first hydration shell, followed by a lower and broader second peak, is observed. A tall, sharp peak in $g_{Ca-O}(r)$ corresponding to the first hydration shell, followed by a lower and broader second peak, is observed. The behavior of $g_{Ca-H}(r)$ is similar to $g_{Ca-O}(r)$ but much broader. The heights of the peaks for both $g_{Ca-O}(r)$ and $g_{Ca-H}(r)$ decrease with water density. In comparison between the RPOL and SPC/E models, the heights of those peaks are slightly higher for $g_{Ca-O}(r)$ but slightly lower for $g_{Ca-H}(r)$, and the locations of those peaks are slightly closer to the origin due to the electronic polarization of the ions and water molecules. This behavior was also observed in the comparison of these two models for Na + at 298 and 683 K in other MD simulation study [45]. For Cl^- ion, the ion–oxygen $g_{Cl-O}(r)$ has nearly only one peak unlike in the case of Ca^{2+}, while the ion–hydrogen $g_{Cl-H}(r)$ is consisted of two peaks as in the cases of Ca^{2+}. The peak heights of $g_{Cl-O}(r)$ and $g_{Cl-H}(r)$ in SPC/E model are much higher than the RPOL model, although the locations of the peaks seem to be almost non-affected.

Table III contains the positions and magnitudes of the maxima and minima of $g_{i-O}(r)$ and $g_{i-H}(r)$ radial distribution functions for Ca^{2+} and Cl^- at 298 K and 673 K using the RPOL and SPC/E models. The value of $g_{i-O}(r)$ for Ca^{2+} for SPC/E model at 298 K is a little different from that for Ca^{2+} at the same temperature in a previous MD simulation [12]: 2.45 A and 14.1 at 1st max., 3.39 A and 0.01 at 1 min, and 4.46 A and 1.96 at 2nd max. for r_{i-O} and g_{i-O}, respectively, although the Lennard-Jones parameters for Ca^{2+} ion–oxygen

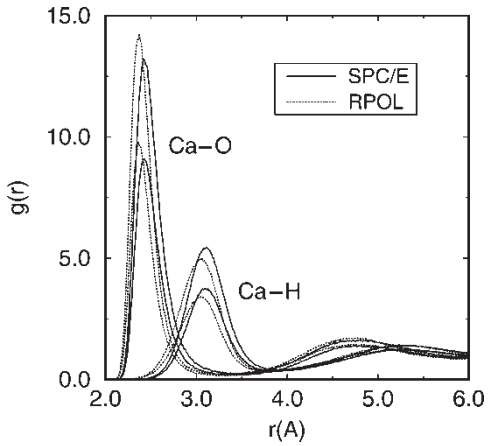

FIGURE 2 Ion–oxygen $g_{i-O}(r)$ and ion–hydrogen $g_{i-H}(r)$ radial distribution functions for Ca^{2+} ion at 673 K over the water densities of 0.60 g/cc (upper curves) and 0.90 g/cc (lower curves).

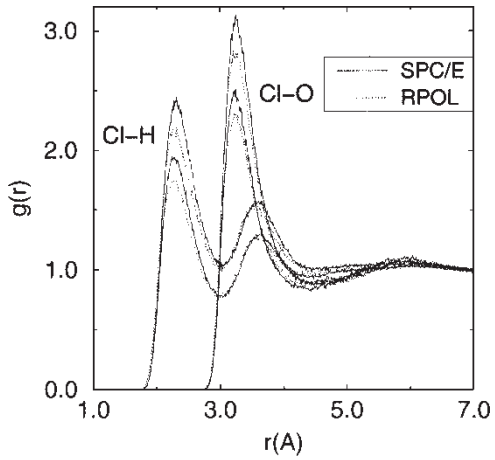

FIGURE 3 Ion–oxygen $g_{i-O}(r)$ and ion–hydrogen $g_{i-H}(r)$ radial distribution functions for Cl^- ion at 673 K over the water densities of 0.60 g/cc(upper curves) and 0.90 g/cc (lower curves).

TABLE III Positions (A) and magnitudes at maxima and minima of $g_{i-O}(r)$ and $g_{i-H}(r)$ radial distribution functions at 673 K for the SPC/E (upper) and RPOL (lower) models

		$g_{i-O}(r)$						$g_{i-H}(r)$					
		1st max.		*1st min.*		*2nd max*		*1st max.*		*1st min.*		*2nd max.*	
Ion	*ρ (g/cc)*	r_{i-O}	g_{i-O}	r_{i-O}	g_{i-O}	r_{i-O}	g_{i-O}	r_{i-H}	g_{i-H}	r_{i-H}	g_{i-H}	r_{i-H}	g_{i-H}
Ca^{2+}	*	2.45	12.9	3.28	0.02	4.69	1.8	3.12	5.1	3.75	0.1	5.25	1.4
	0.60	2.43	13.3	3.35	0.3	4.78	1.7	3.12	5.5	3.91	0.4	5.25	1.4
	0.75	2.42	10.8	3.36	0.2	4.80	1.4	3.12	4.4	3.90	0.4	5.27	1.3
	0.90	2.43	9.1	3.38	0.2	4.81	1.4	3.11	3.8	3.90	0.3	5.38	1.2
Cl^-	*	3.21	3.6	3.87	0.5	5.06	1.2	2.23	3.3	3.03	0.3	3.68	1.6
	0.60	3.23	3.1	4.40	0.9	5.79	1.1	2.29	2.4	3.01	1.0	3.60	1.6
	0.75	3.23	2.7	4.40	0.9	5.79	1.1	2.30	2.1	3.01	0.9	3.60	1.4
	0.90	3.23	2.5	4.40	0.8	5.79	1.1	2.29	2.0	3.01	0.8	3.60	1.3
Ca^{2+}	*	2.36	13.5	3.19	0.01	4.58	1.8	3.04	4.3	3.59	0.1	5.26	1.4
	0.60	2.37	14.2	3.28	0.2	4.77	1.7	3.06	5.0	3.85	0.4	5.27	1.4
	0.65	2.37	13.2	3.28	0.2	4.76	1.6	3.05	4.6	3.85	0.4	5.27	1.4
	0.70	2.37	12.4	3.28	0.2	4.78	1.6	3.04	4.3	3.86	0.4	5.26	1.3
	0.75	2.37	11.5	3.28	0.2	4.76	1.5	3.04	4.0	3.84	0.3	5.26	1.3
	0.80	2.37	10.9	3.28	0.2	4.77	1.5	3.04	3.8	3.84	0.3	5.25	1.3
	0.85	2.37	10.2	3.28	0.2	4.78	1.5	3.05	3.6	3.82	0.3	5.26	1.3
	0.90	2.36	9.8	3.28	0.2	4.77	1.5	3.05	3.4	3.82	0.4	5.25	1.3
Cl^-	*	3.19	3.1	3.94	0.6	5.14	1.2	2.22	2.8	3.03	0.3	3.60	1.4
	0.60	3.24	2.9	4.40	0.9	5.81	1.1	2.29	2.2	3.03	1.0	3.59	1.5
	0.65	3.23	2.7	4.40	0.9	5.85	1.1	2.30	2.1	3.04	1.0	3.59	1.5
	0.70	3.22	2.6	4.41	0.9	5.85	1.1	2.30	2.0	3.03	0.9	3.60	1.4
	0.75	3.22	2.5	4.39	0.9	5.86	1.1	2.30	1.9	3.03	0.9	3.59	1.4
	0.80	3.23	2.4	4.40	0.9	5.87	1.1	2.30	1.8	3.02	0.8	3.58	1.3
	0.85	3.24	2.3	4.40	0.9	5.87	1.1	2.30	1.8	3.04	0.8	3.60	1.3
	0.90	3.23	2.3	4.41	0.9	5.88	1.1	2.30	1.7	3.01	0.8	3.60	1.3

* 298 K and 0.997 g/cc.

interaction are equal. The change of these values in the RPOL model is the same as in the cases at 673 K discussed above. The heights of the first peaks for both $g_{Ca-O}(r)$ and $g_{Ca-H}(r)$ for both models decrease as water density decreases. For $g_{Cl-O}(r)$ and $g_{Cl-H}(r)$ at 298 K, the locations of the first peaks for the RPOL model are also slightly closer to the origin than for SPCE model but the difference is very small and the peak heights of $g_{Cl-O}(r)$ and $g_{Cl-H}(r)$ in the RPOL model are much lower than those in SPC/E model. At supercritical temperature (673 K), the differences in two models are even smaller.

Some thermodynamic and structural quantities have been calculated and listed in Table IV. The average ion–water potential energies, Eq. (2), for Ca^{2+} and Cl^- for both the RPOL and SPC/E models increases negatively with increasing water density as was observed in all the previous MD simulations for ion–water systems at supercritical state [4,13,14,17]. This is easily understood from the point of view that the number of water around an ion is increased with increasing water density as seen in the hydration number in Table IV. The decrease of this ion–water energy on changing from the SPC/E to the RPOL model is significantly large, which seems related to the electronic polarization of the ions and water molecules. In the RPOL model, the induced dipole moment and the polarization energy, Eq. (3), for Ca^{2+} decreases with increasing water density but for Cl^-, the opposite is observed. Note that the magnitudes of the induced dipole moment and the polarization energy of Cl^- are 8 and 11 times as large as those of Ca^{2+}, respectively, which is mainly originated from the large polarizability of Cl^-. Those values for the oxygen and the hydrogen of water always increase with water density. This behavior of the induced dipole moment and the polarization energy of cation and water as a function of water density at 673 K was also observed in the previous MD simulations for Li + in the RPOL models for both with and without the 3-body interaction [17]. When the temperature is lowered from 673 to 298 K, or when water density is raised from 0.60–0.90 to 0.997 g/cc, the same effect on the induced dipole moment and the polarization energy for Ca^{2+}, Cl^-, and water with increasing water density is observed.

The decrement in the induced dipole moment implies the increment in the spherical symmetry of charge distribution around an ion or atom. What causes the increment (decrement) in the spherical symmetry of charge distribution around Ca^{2+} (Cl^-) by increasing water density? The SPC/E and RPOL models have a significant amount of charge asymmetry and as a result, the orientations of the water molecules in the first hydration shell of a cation and an anion are different. For a cation, the oxygen atoms of water molecules in the first hydration shell are closer to the ion and are pointed

TABLE IV Average ion–water potential energy (kJ/mol), polarization energies Eq. (3) of ion and water, induced dipole moments (*Debye*) of ion and water, hydration number (n), and ionic potential energy divided by the hydration number at 673 K for the SPC/E (uppper) and RPOL(lower) models

Ion	ρ *(g/cc)*	$-U_{i-w}$	$-U_{pol}$ *(ion)*	$-U_{pol}$ *(H_2O)*	μ *(ion)*	$\mu_O(H_2O)$	$\mu_H(H_2O)$	n	$-U_{ion}$
Ca^{2+}	*	2437(7)	–	–	–	–	–	7.93	307(1)
	0.60	2224(8)	–	–	–	–	–	7.42	300(1)
	0.75	2244(9)	–	–	–	–	–	7.51	299(1)
+	0.90	2270(9)	–	–	–	–	–	7.67	296(1)
Cl^-	*	535(4)	–	–	–	–	–	7.50	71.3(5)
	0.60	460(5)	–	–	–	–	–	8.17	56.3(6)
	0.75	472(5)	–	–	–	–	–	8.72	54.1(6)
	0.90	483(5)	–	–	–	–	–	9.80	49.3(5)
Ca^{2+}	*	1822(8)	0.323(26)	13.1(5)	0.077(3)	0.372(3)	0.130(1)	6.57	277(1)
	0.60	1768(9)	0.630(53)	4.82(3)	0.107(5)	0.200(1)	0.068(4)	6.58	269(1)
	0.65	1771(9)	0.628(52)	5.12(3)	0.106(5)	0.208(1)	0.071(4)	6.65	266(1)
	0.70	1773(8)	0.625(53)	5.44(3)	0.106(5)	0.216(1)	0.074(5)	6.68	265(1)
	0.75	1778(10)	0.621(52)	5.79(3)	0.106(5)	0.225(1)	0.077(5)	6.71	265(1)
	0.80	1781(10)	0.618(52)	6.15(4)	0.105(5)	0.234(1)	0.080(5)	6.75	264(1)
	0.85	1786(10)	0.611(51)	6.53(4)	0.105(5)	0.243(2)	0.084(5)	6.84	261(1)
	0.90	1790(10)	0.610(51)	6.94(4)	0.105(5)	0.252(2)	0.087(4)	6.88	260(1)
Cl^-	*	397(4)	8.83(66)	12.6(5)	0.994(42)	0.371(4)	0.131(4)	7.16	56.7(7)
	0.60	369(5)	6.44(52)	3.91(3)	0.837(37)	0.187(1)	0.066(5)	8.10	46.3(7)
	0.65	371(5)	6.61(53)	4.23(3)	0.849(37)	0.196(2)	0.069(5)	8.35	45.2(6)
	0.70	372(5)	6.63(54)	4.58(3)	0.849(37)	0.205(2)	0.072(5)	8.60	44.0(6)
	0.75	374(5)	6.77(55)	4.93(3)	0.857(38)	0.214(2)	0.076(5)	8.90	42.8(5)
	0.80	376(5)	6.91(56)	5.31(3)	0.867(47)	0.223(2)	0.079(6)	9.20	41.6(5)
	0.85	377(5)	7.28(58)	5.71(3)	0.889(47)	0.233(2)	0.082(6)	9.53	40.3(5)
	0.90	377(5)	7.60(61)	6.13(4)	0.910(47)	0.242(2)	0.086(6)	9.71	39.6(5)

$U_{pol}(H_2O)$ is divided by the number of water molecules ($N = 215$) and $U_{ion} = U_{i-w} + U_{pol}(ion)$. Uncertainties in the last reported digit(s) are given in parenthesis. *298 K and 0.997 g/cc.

towards it, while for an anion, one of the hydrogen atoms of a water molecule in this shell is closer than the oxygen atom of same water molecule and is pointed towards the ion. From this view of point, a positive ion constructs the symmetry of charge distribution of water molecules in the first hydration shell, whereas a negative ion does the asymmetry of charge distribution in this shell. Increasing water density enhances the constructions of the symmetry for the positive ion and asymmetry for the negative ion of charge distribution in this shell.

The hydration number n is defined by integrating the ion–oxygen radial distribution function $g_{i-O}(r)$ from the inner to the outer boundary of the first hydration shell:

$$n = 4\pi\rho\int_0^{r_{\min}} g_{iO}(r)\, r^2\, dr \qquad (9)$$

where ρ is the number density of bulk water and $r_{\min}$ is the point at which the first minimum in $g_{i-O}(r)$ occurs. Table IV contains the hydration number of water in the first hydration shell around Ca^{2+} and Cl^- ions. The hydration numbers reported by other MD studies are 9.2 [30] at 300 K and 7.9 [12] at 298 K around Ca^{2+}. The latter value is essentially equal to the result in the present study. The significant decrease of this number for Ca^{2+} at 298 and 673 K on changing from the SPC/E to the RPOL model is a contrast to almost non-factor for Cl^- at the same temperatures. When the temperature is lowered from 673 to 298 K, this number around Cl^- decreases for both models while for Ca^{2+} case, it is slightly increased for the SPC/E model or almost non-factor for the RPOL model.

The potential energy per hydration water molecule, defined as the average ion–water potential energy divided by the hydration number, for Ca^{2+} and Cl^- ions is also listed in Table IV. These energies for the SPC/E and RPOL models are slightly increased as water density decreases over the whole range of water density considered (0.60–0.90 g/cc). In the study of the limiting conductances of NaCl, LiCl, NaBr, and CsBr by MD simulations using the SPC/E model, it was found that the effect of the number of hydration water molecules around ions dominates in the higher-density region (0.48–0.74 g/cc) while the interaction between the ions and the hydration water molecules (as measured by the potential energy per hydration water molecule) dominates in the lower-density region (0.22–0.40 g/cc). In the present study for the water density of 0.60–0.90 g/cc, the latter factor in the lower-density region is not as dominant as in the cases of Na + and Cl^-. The small changes in the average ion–water potential energies and the hydration numbers for Ca^{2+} with water density is notable. The small change in the energetics of Ca^{2+} and the structure of water around the ion suggests that the chemical circumstances around these ions is almost invariable over the whole range of water density considered, and this is mainly due to the strong divalent ion–water interaction unlike in the cases of monovalent ions. The Ca^{2+} ion and water molecules in the first hydration shell moving together as an entity interacts with the second hydration shell

water molecules (a solventberg picture). The same kind of behavior for divalent ions (Na^{2+} and Cl^{2-}) over the water density of 0.48–0.74 g/cc was already observed in a previous study [8].

Chemical circumstance of water molecules around an ion plays an important role to investigate the dynamics of the ion. Especially, hydrogen bonds between water molecules in the first hydration shell around the ion determine ionic mobility. The breaking of hydrogen bonds, for example, results in an increase of ionic mobility. Hydrogen-bond auto-correlation function provides an important information of the stability of the hydrogen bond. The definition of hydrogen bond is given by Luzar and Chandler [46,47]: a pair of water molecules is hydrogen bonded when the following criteria are satisfied.

(1) The inter-oxygen distance is less than 3.60 A.
(2) The O–H distance between the bonded molecules is less than 2.45 A.
(3) The O–H–O angle is less than 30°.

A hydrogen-bond population operator $h(t)$ is defined by Luzar and Chandler [46], as 1 if a pair of water molecules is hydrogen bonded and 0 otherwise. The persistence of hydrogen bonding is measured by the time auto-correlation function

$$c(t) = \frac{\langle h(t)h(0)\rangle}{\langle h\rangle} \tag{10}$$

where $\langle h\rangle$ is the time average of $h(t)$; the average number of intermolecular hydrogen bonds in a water molecule. We plotted the hydrogen-bond correlation functions of water molecules in the first hydration shell around Ca^{2+} and Cl^- ions, and of bulk water at 298 and at 673 K for the SPC/E and RPOL models at the water densities of 0.60, 0.75 and 0.90 g/cc in Figs. 4–7. At the first glance, hydrogen-bond correlations around two ions show a significant difference for both models at both temperatures of the system. Hydrogen bonding around Ca^{2+} ion persists longer than in bulk water except at the very initial time whereas the opposite is observed for the case of Cl^- ion. This suggests that the structure of water molecules around a positive ion favors the formation of hydrogen bonding whereas it does not for a negative ion.

In comparison of Figs. 4 and 5, the bulk water of the RPOL model shows slightly greater hydrogen bonding than the SPC/E model at 298 K but slightly less hydrogen bonding at 673 K. For water molecules in the first hydration shell around Ca^{2+} ion, hydrogen bonding of the RPOL model persists longer than the SPC/E model for the initial time up to 6 ps at 298 K. At 673 K hydrogen bonding of water molecules of the SPC/E model in the first hydration shell around Ca^{2+} ion increases with water density,

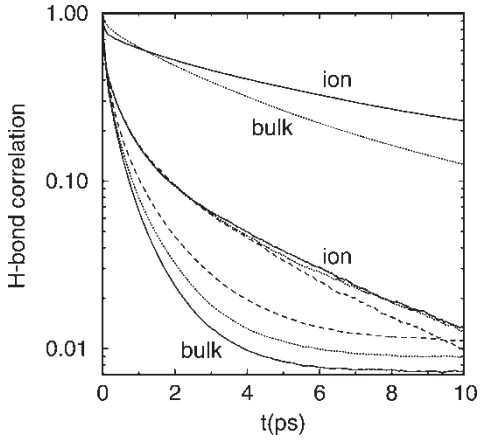

FIGURE 4 H-bond correlation functions of water molecules in the first hydration shell around Ca^{2+} ion and of bulk water at 298 K(upper) and at 673 K(lower) for the SPC/E model (solid line : 0.60 g/cc, dotted line : 0.75 g/cc, and dashed line : 0.90 g/cc).

but the dramatically opposite behavior is observed for the RPOL model. This implies that at 298 K the electronic polarization around the ion leads to an adjustment of the dipole moment of water molecules in the first hydration shell and results in the strengthening of the hydrogen bonds between water molecules around the ion. Similarly, at 673 K, the polarization energy of Ca^{2+} ion decreases with water density, which results in the weakening of hydrogen bonding between water molecules around the ion with water density. In Figs. 6 and 7, hydrogen-bond correlations of water molecules around Cl^- ion and of bulk water at both temperatures are nearly unchanged by the electronic polarization. At 673 K, hydrogen bonding of water molecules around Cl^- ion and of bulk water for both models persists longer as water density increases. The effect of the electronic polarization causes a slightly decrease in hydrogen bonding, which is

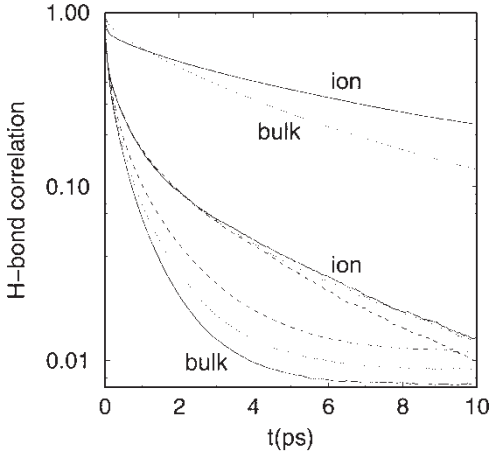

FIGURE 5 H-bond correlation functions of water molecules in the first hydration shell around Ca^{2+} ion and of bulk water at 298 K (upper) and at 673 K (lower) for the RPOL model(solid line : 0.60 g/cc, dotted line : 0.75 g/cc, and dashed line : 0.90 g/cc).

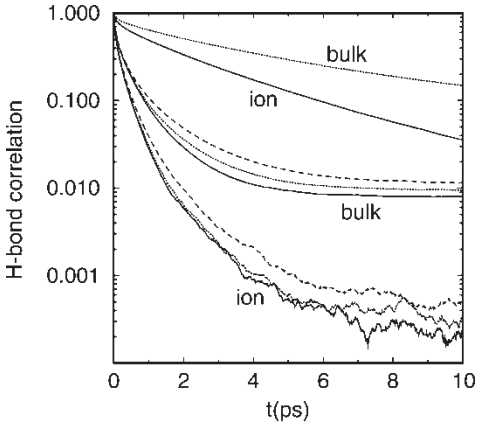

FIGURE 6 H-bond correlation functions of water molecules in the first hydration shell around Cl^- ion and of bulk water at 298 K (upper) and at 673 K (lower) for the SPC/E model(solid line : 0.60 g/cc, dotted line : 0.75 g/cc, and dashed line : 0.90 g/cc).

consistent with the increase of the polarization energy of Cl^- with water density.

The diffusion coefficients Di of Ca^{2+} and Cl^-, calculated from the mean square displacements (MSD) and from the velocity auto-correlation functions (VAC) using the SPC/E and RPOL models, are listed in Table V and the limiting conductances λ^o determined from the diffusion coefficients are also listed in the same table. The limiting conductances of $CaCl_2$ obtained from those of the individual ions by $\lambda^o = \lambda^o_{2+} + 2\lambda^o_-$ are compared with the experimental results in Fig. 1 over the whole range of water density considered, which exhibit a linear dependence on water density for both models. Note that the significant increase of the limiting conductances for Ca^{2+} and Cl^- ions at 298 and 673 K on changing from the SPC/E to the RPOL model. This is mainly due to the weakening in the ion–water potential energy for Ca^{2+} and Cl^- ions as listed in Table V, which is caused by the electronic polarization. As shown in Table I, the change from the SPC/E to the RPOL model is accompanied with the change of LJ parameters for Cl^- ion but not for Ca^{2+} ion. For the case of Ca^{2+}, therefore, the electronic polarization causes a decrease in the ion–water potential energy and an increase in the limiting conductances of Ca^{2+} ion, and for Cl^-, it is believed that the slight change of LJ parameters also affects the ion–water potential energy but the main reason for this energy change is due to the electronic polarization.

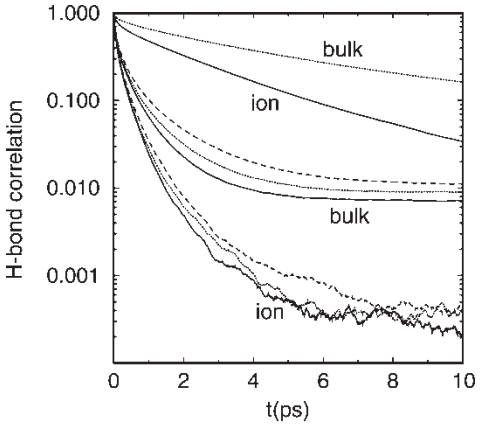

FIGURE 7 H-bond correlation functions of water molecules in the first hydration shell around Cl^- ion and of bulk water at 298 K (upper) and at 673 K (lower) for the RPOL model (solid line : 0.60 g/cc, dotted line : 0.75 g/cc, and dashed line : 0.90 g/cc).

TABLE V Diffusion coefficient $D_i(10^{-5}cm^2/s)$ and molar conductance $\lambda^o_i(S{\cdot}cm^2/mol)$ of Ca^{2+} and Cl^- at infinite dilution in supercritical water at 673 K calculated from mean square displacement (MSD) and velocity autocorrelation function (VAC) for the SPC/E (upper) and RPOL (lower) models

		D_i		λ^o_i	
Ion	*ρ (g/cc)*	*MSD*	*VAC*	*MSD*	*VAC*
Ca^{2+}	*	0.88(14)	0.91(17)	132(21)	137(26)
	0.60	18.4(26)	18.0(40)	1220(173)	1200(266)
	0.75	14.8(24)	14.6(25)	988(160)	971(166)
	0.90	11.6(13)	11.7(22)	772(87)	779(146)
Cl^-	*	2.03(33)	2.04(45)	86.4(124)	76.6(169)
	0.60	38.5(62)	38.8(65)	640(103)	645(108)
	0.75	33.4(30)	33.6(44)	556(50)	559(73)
	0.90	25.7(27)	25.2(35)	427(45)	419(58)
Ca^{2+}	*	0.96(18)	1.04(28)	144(27)	156(42)
	0.60	18.8(30)	19.4(29)	1250(200)	1290(193)
	0.65	17.1(18)	17.4(20)	1140(120)	1160(133)
	0.70	16.5(21)	16.4(20)	1100(140)	1090(133)
	0.75	15.4(28)	15.3(34)	1020(186)	1020(226)
	0.80	14.2(21)	13.7(23)	945(140)	912(153)
	0.85	13.2(20)	13.0(21)	878(133)	865(140)
	0.90	12.2(15)	12.0(22)	812(100)	798(146)
Cl^-	*	3.13(53)	3.21(65)	117(20)	121(24)
	0.60	40.6(57)	40.3(67)	675(95)	670(111)
	0.65	38.5(65)	37.1(76)	640(80)	617(126)
	0.70	36.7(52)	36.9(70)	610(87)	614(116)
	0.75	35.3(48)	35.3(63)	587(80)	587(105)
	0.80	32.4(41)	32.5(57)	538(68)	541(95)
	0.85	29.5(33)	27.5(43)	491(55)	457(72)
	0.90	27.4(50)	27.5(56)	456(83)	458(93)

Uncertainties in the last reported digit(s) are given in parenthesis. *298 K and 0.997 g/cc.

The monotonous decrement of the limiting conductances of divalent ions with water density were already seen for Na^{2+} and Cl^{2-} over the water density of 0.48–0.74 g/cc in a previous study [8] and for Mg^{2+} and Ca^{2+} over the water density of 0.60–0.90 g/cc in a previous study [4]. A possible explanation for this may be the strong Coulomb interaction of the divalent ions with the hydration water molecules. Between two important competing factors in the explanation of the limiting conductances of LiCl, NaCl, NaBr, and CsBr in supercritical water at 673 K [13,14], the effect of the ion–water interaction strength becomes non-factor against the other effect which is that of the number of hydration water molecules around ions. From the view of the solventberg picture of these ions, the ion and its shell moving together as an entity interacts with the second hydration shell water molecules, and its mobility is restricted mostly by the number of the second hydration shell water which is proportional

to water density of the whole system. The electronic polarization effect causes an increase in the limiting conductances of Ca^{2+} by weakening the ion–water potential energy.

The calculated limiting conductances of Cl^- for the SPC/E model over the whole range of water density(0.60–0.90 g/cc) is consistent with those over the water density of 0.22–0.74 g/cc in the previous study [13]. The range of water density considered in this study belongs to the higher-density region (above 0.45 g/cc) in which the effect of the number of hydration water molecules around ions dominated [13]. As water density increases, the water molecules of the first hydration shell restrict the mobility of Cl^- and the limiting conductances of Cl^- decrease nearly linearly. By employing the RPOL model for ion and water molecules, the limiting conductances for Cl^- is also increased by weakening the ion–water potential energy.

CONCLUDING REMARKS

In this study, we have extended our MD simulations of the systems to Ca^{2+} and Cl^- in ambient and supercritical states using the SPC/E and RPOL models for ions and water molecules. The effect of the electronic polarization on the structural properties of water molecules around the ions causes a slight increase in the first peak for $g_{Ca-O}(r)$ but a slight decrease for $g_{Ca-H}(r)$, and a slight approach to the origin in the locations of those peaks for Ca^{2+}. The peak heights of $g_{Cl-O}(r)$ and $g_{Cl-H}(r)$ in RPOL model are much lower than the SPC/E model, although the locations of the peaks seem to be almost non-affected. The induced dipole moment and the polarization energy for Ca^{2+} decreases with increasing water density but for Cl^- and atoms of water molecule, the opposite is observed, which is related to the charge distribution of water molecules in the first hydration shell around the ions. An analysis of hydrogen-bond correlations shows that hydrogen bonding around Ca^{2+} ion persists longer than in bulk water except at the very initial time whereas the opposite is observed for the case of Cl^- ion. This suggests that the structure of water molecules around a positive ion favors the formation of hydrogen bonding whereas it does not for a negative ion. At 673 K hydrogen bonding of water molecules of the SPC/E model in the first hydration shell around Ca^{2+} ion increases with water density, but the dramatically opposite behavior is observed for the RPOL model. This implies that the polarization energy of Ca^{2+} ion decreases with water density, which results in the weakening of hydrogen bonding between water molecules around the ion with water density. Hydrogen-bond correlations of water molecules around Cl^- ion and of bulk water at both temperatures are nearly unchanged by the electronic polarization. At 673 K, hydrogen bonding of water molecules around Cl^- ion and of bulk water for both models persists longer as water density increases. The effect of the electronic polarization causes a slightly decrease in hydrogen bonding, which is consistent with the increase of the polarization energy of Cl^- with water density. The most significant effect of the electronic polarization is appeared in a decrease in the ion–water potential energy and, as a result, an increase in the limiting conductances for both ions. The limiting conductances of $CaCl_2$ obtained for both models exhibit a linear dependence on water density. In the lower water density region of 06–0.7 g/cc in this study, the effect of the electronic polarization is too small to cause a deduction in the limiting conductances for both ions. The application of Ewald summation to the use of the RPOL model for ions and water molecules in dilute aqueous solutions of $CaCl_2$ may be indispensable.

Acknowledgements

This research was supported by the Provincial University Support Research Fund of the Korea Science and Engineering Foundation (KOSEF), 2000.

References

[1] Zimmerman, G.H., Gruszkiewicz, M.S. and Wood, R.H. (1995) "New apparatus for conductance measurements at high temperatures: conductance of aqueous solutions of LiCl, NaCl, NaBr, and CsBr at 28 MPa and water densities from 700 to 260 $kg{\cdot}m^{-3}$", *J. Phys. Chem.* **99**, 11612.
[2] Ho, P.C. and Palmer, D.A. (1996) "Ion association of dilute aqueous sodium hydroxide solutions to 600°C and 300 MPa by conductance measurements", *J. Solution Chem.* **25**, 711.
[3] Frantz, J.D. and Marshall, W.L. (1982) "Electrical conductances and ionization constants of calcium chloride and magnesium chloride in aqueous solutions at temperatures to 600°C and pressures to 400 bars", *Am. J. Sci.* **282**, 1666.
[4] Lee, S.H. (2004) "Molecular dynamics simulation of the limiting conductance of $MgCl_2$ and $CaCl_2$ in supercritical water using SPC/E model for water", *Mol. Sim.* **30**, 37.
[5] Berendsen, H.J., Grigera, C.J.R. and Straatsma, T.P. (1987) "The missing term in effective pair potentials", *Phys. Chem.* **91**, 6269.
[6] Dang, L.X. (1992) "The nonadditive intermolecular potential for water revised", *J. Chem. Phys.* **97**, 2659.
[7] Smith, D.E. and Dang, L.X. (1994) "Computer simulations of NaCl in polarizable water", *J. Chem. Phys.* **100**, 3757.
[8] Lee, S.H. and Cummings, P.T. (2001) "Molecular dynamics simulation of the limiting conductance for Na^{2+}, Cl^{2-}, Na^0, and Cl^0 in supercritical water", *Mol. Sim.* **27**, 199.
[9] De Leeuw, S.W., Perram, J.W. and Smith, E.R. (1980) "Simulation of electrostatic systems in periodic boundary conditions. I. Lattice sums and dielectric constant", *Proc. R. Soc. Lond.* **A373**, 27.
[10] Lee, S.H. and Rasaiah, J.C. (1994) "Molecular dynamics simulation of ionic mobility. I. Alkali metal cations in water at 25°C", *J. Chem. Phys.* **101**, 6964.
[11] Lee, S.H. and Rasaiah, J.C. (1996) "Molecular dynamics simulation of ionic mobility. 2. Alkali metal and halide ions using the SPC/E model for water at 25°C", *J. Phys. Chem.* **100**, 1420.

[12] Koneshan, S., Rasaiah, J.C., Lynden-Bell, R.M. and Lee, S.H. (1998) "Solvent structure, dynamics, and ion mobility in aqueous solutions at 25°C", *J. Phys. Chem.* **B 102**, 4193.
[13] Lee, S.H., Cummings, P.T., Simonson, J.M. and Mesmer, R.E. (1998) "Molecular dynamics simulation of the limiting conductance of NaCl in supercritical water", *Chem. Phys. Lett.* **293**, 289.
[14] Lee, S.H. and Cummings, P.T. (2000) "Molecular dynamics simulation of the limiting conductance of LiCl, BaBr, and CsBr in supercritical water", *J. Chem. Phys.* **112**, 864.
[15] Lee, S.H. (2001) "Preliminary molecular dynamics simulations of the OSS2 model for the solvated proton in water", *Bull. Kor. Chem. Soc.* **22**, 847.
[16] Lee, S.H. (2002) "Molecular dynamics simulations of the OSS2 model for water and oxonium ion monomers, and protonated water clusters", *Bull. Kor. Chem. Soc.* **23**, 107.
[17] Lee, S.H. (2003) "Molecular dynamics simulation of the limiting conductance of Li^+ ion in supercritical water using polarizable models", *Mol. Sim.* **29**, 211.
[18] Applequist, J., Carl, J.R. and Fung, K.-K. (1972) "An atom dipole interaction model for molecular polarizability. Application to polyatomic molecules and determination of atom polarizabilities", *J. Am. Chem. Soc.* **94**, 2952.
[19] Sangster, M.J.L. and Atwood, R.M.J. (1978) "Interionic potentials for alkali halides: II Completely crystal independent specification of Born-Mayer potentials", *Phys. C: Solid State Phys.* **11**, 1541.
[20] Curtiss, L.A., Hautman, J.W. and Rahman, A. (1987) "Nonadditivity of *ab initio* pair potentials for molecular dynamics of multivalent transition metal ions in water", *J. Chem. Phys.* **86**, 2319.
[21] Foresman, J.B. and Brooks, C.L. (1987) "An *ab initio* study of hydrated chloride ion complexes: evidence of polarization effects and nonadditivity", *J. Chem. Phys.* **87**, 5892.
[22] Corongiu, G., Migliore, M. and Clementi, E. (1989) "Hydration free energy for Li^+ at infinite dilution with a three-body *ab initio* potential", *J. Chem. Phys.* **90**, 4629.
[23] Cieplak, P. and Kollman, P.A. (1990) "Monte Carlo simulation of aqueous solutions of Li^+ and Na^+ using many-body potentials. Coordination number, ion solvation enthalpies, and the relative free energy of solvation", *J. Chem. Phys.* **92**, 6761.
[24] Caldwell, J., Dang, L.X. and Kollman, P.A. (1990) "Implementation of nonadditive intermolecular potentials by use of molecular dynamics: development of a water–water potential and water–ion cluster interactions", *J. Am. Chem. Soc.* **112**, 9144.
[25] Dang, L.X., Rice, J.E., Caldwell, J. and Kollman, P.A. (1991) "Ion solvation in polarizable water: molecular dynamics simulations", *J. Am. Chem. Soc.* **113**, 2481.
[26] Perera, L. and Berkowitz, M.L. (1991) "Many-body effects in molecular dynamics simulations of $Na^+(H_2O)_n$ and $Cl^-(H{-}2O)_n$", *J. Chem. Phys.* **95**, 1954.
[27] Dang, L.X. (1992) "Development of nonadditive intermolecular potentials using molecular dynamics: solvation of Li^+ and F^- ions in polarizable water", *J. Chem. Phys.* **96**, 6970.
[28] Dang, L.X. and Garrett, B.C. (1993) "Photoelectron spectra of the hydrated iodine anion from molecular dynamics simulations", *J. Chem. Phys.* **99**, 2972.
[29] Dang, L.X. and Smith, D.E. (1993) "Molecular dynamics simulations of aqueous ionic clusters using polarizable water", *J. Chem. Phys.* **99**, 6950.
[30] Probst, M.M., Radnai, T., Heinzinger, Z., Bopp, P. and Rode, B.M. (1985) "Molecular dynamics and X-ray investigation of an aqueous $CaCl_2$ solution", *J. Phys. Chem.* **89**, 753.
[31] Perera, L., Essmann, U. and Berkowitz, M.L. (1995) "Effect of the treatment of long-range forces on the dynamics of ions in aqueous solutions", *J. Chem. Phys.* **102**, 450.
[32] Barker, J.A. and Watts, R.O. (1973) "Monte Carlo studies of the dielectric properties of water-like models", *Mol. Phys.* **26**, 789.
[33] Reid, R.C., Prausnitz, J.M. and Sherwood, T.K. (1977) *The Properties of Liquids and Gases* (McGraw-Hill, New York).
[34] Guissani, Y. and Guillot, B. (1993) "A computer simulation study of the liquid–vapor coexistence curve of water", *J. Chem. Phys.* **98**, 8221.
[35] Simmons, A.D. and Cummings, P.T. (1986) "Non-equilibrium molecular dynamics simulation of dense fluid methane", *Chem. Phys. Lett.* **129**, 92.
[36] Hoover, W.G., Ladd, A.J.C. and Moran, B. (1982) "High strain rate plastic flow studied via nonequilibrium molecular dynamics", *Phys. Rev. Lett.* **48**, 1818.
[37] Evans, D.J. (1983) "Computer experiment for nonlinear thermodynamics of Couette flow", *J. Chem. Phys.* **78**, 3297.
[38] Evans, D.J., Hoover, W.G., Failor, B.H., Moran, B. and Ladd, A.J.C. (1983) "Nonequilibrium molecular dynamics via Gauss's principle of least constraint", *Phys. Rev. A.* **28**, 1016.
[39] Evans, D.J. (1977) "On the representation of orientation space", *Mol. Phys.* **34**, 317.
[40] Evans, D.J. and Murad, S. (1977) "Singularity free algorithm for molecular dynamics simulation of rigid polyatomics", *Mol. Phys.* **34**, 327.
[41] Gear, C.W. (1971) *Numerical Initial Value Problems in Ordinary Differential Equation* (Prentice-Hall, Englewood Cliffs, NJ).
[42] Evans, D.J. and Morriss, G.P. (1984) "Non-Newtonian molecular dynamics", *Comput. Phys. Rep.* **1**, 297.
[43] Steinhauser, O. (1982) "Reaction field simulation of water", *Mol. Phys.* **45**, 335.
[44] Lide, D.R. (20022003) *CRC Handbook of Chemistry and Physics*, 83rd Ed. (CRC Press Inc., Boca Raton), pp 12–18.
[45] Koneshan, S., Rasaiah, J.C. and Dang, L.X. (2001) "Computer simulation studies of aqueous solutions at ambient and supercritical conditions using effective pair potential and polarizable potential models for water", *J. Chem. Phys.* **B 102**, 7544.
[46] Luzar, A. and Chandler, D. (1996) "Hydrogen-bond kinetics in liquid water", *Nature (Lond.)* **379**, 55.
[47] Luzar, A. and Chandler, D. (1996) "Effect of environment on hydrogen bond dynamics in liquid water", *Phys. Rev. Lett.* **36**, 928.